

# Systematic Errors in the Estimation of Black Hole Masses by Reverberation Mapping

Julian H. Krolik

*Department of Physics and Astronomy, Johns Hopkins University, Baltimore, MD 21218*

## ABSTRACT

The mass of the central black hole in many active galactic nuclei has been estimated on the basis of the assumption that the dynamics of the broad emission line gas are dominated by the gravity of the black hole. The most commonly-employed method is to estimate a characteristic size-scale  $r_*$  from reverberation mapping experiments and combine it with a characteristic velocity  $v_*$  taken from the line profiles; the inferred mass is then estimated by  $r_*v_*^2/G$ . We critically discuss the evidence supporting the assumption of gravitational dynamics and find that the arguments are still inconclusive. We then explore the range of possible systematic error if the assumption of gravitational dynamics is granted. Inclination relative to a flattened system may cause a systematic underestimate of the central mass by a factor  $\sim (h/r)^2$ , where  $h/r$  is the aspect ratio of the flattening. The coupled effects of a broad radial emissivity distribution, an unknown angular radiation pattern of line emission, and sub-optimal sampling in the reverberation experiment can cause additional systematic errors as large as a factor of 3 or more in either direction.

## 1. Introduction

The constant variability of AGN lends itself to employment as a diagnostic of their internal structure. Most notably, because the ionizing continuum drives the optical/UV emission lines, the time-lag between fluctuations in the continuum and fluctuations in the lines can be used to constrain the distance between the two emission regions under the assumption that it simply represents light travel-time. This program, called “reverberation mapping” by analogy with the seismic techniques used in oil exploration, has been extensively implemented, especially in the past decade (see, for example, the reviews in Gondhalekar et al. 1994).

Recently there have been a number of attempts to combine reverberation-mapping measurements of the broad emission line size scale  $r_*$  with spectroscopic measurements of the line width  $v_*$  in order to estimate the mass of the central black hole (Ho 1999, Wandel et al. 1999; Kaspi et al. 2000). These two quantities can be combined to determine the central mass if the spread of projected velocities seen in the line width is due to motions controlled by the gravity of the central black hole. If that is the case, the central mass  $M \sim r_*v_*^2/G$ .

The logic of the argument depends crucially on our confidence that gravity truly dominates the dynamics of the emission line material. If the estimate  $M \sim r_* v_*^2 / G$  is to be meaningful, we must be able to rule out significant influence from other forces such as radiation pressure or magnetic fields. The quality of the evidence so far will be discussed in §II.

If we grant that gravity is the most important force, the next step is to change the “ $\sim$ ” in the relation to an “ $=$ ”; i.e., writing  $M = q r_* v_*^2 / G$ , we must evaluate the coefficient  $q$  as accurately as possible. In many efforts hitherto (e.g. Wandel et al. 1999, Kaspi et al. 2000),  $q$  has been implicitly taken to be the value appropriate to sources following isotropically-oriented circular orbits at radius  $r_*$ . This value is designated the “virial” mass. As we shall show, however, there can be a sizable ratio between the true mass and this “virial” estimate. Several factors combine to determine this ratio. Many of these have been mentioned and discussed qualitatively in the literature (e.g., Wandel et al. 1999, Kaspi et al. 2000), but few have been studied quantitatively. A proper evaluation of the relation between the “virial” mass and the true mass is important because the “virial” mass is often compared with other mass estimates (Ho 1999; Wandel 1999; Kaspi et al. 2000; Gebhardt et al. 2000c).

The first problem to consider is that there may be a delay between variations in the ionizing continuum (which is genuinely responsible for driving line emission) and the associated variations in the continuum band that is actually observed. Any such delay would artificially enlarge  $r_*$  by an amount equal to  $c$  times the delay. There are some observational indications that delays of this sort exist, but they appear (if real) to be short compared to the continuum–line delay (Collier et al. 1998).

Next, if all the line emission occurred within a thin spherical shell at radius  $r$ , for a fixed definition of  $v_*$  in terms of the line profile, the parameter  $q$  can vary over a wide range depending on the orbital shape distribution and the orbital inclination distribution. This source of systematic error will be discussed in §III.

The detailed nature of internal (i.e., non-kinematic) properties of the emitting matter also influence the parameter  $q$ , so that, in the absence of information constraining these properties, there is an associated systematic error (see, e.g., the qualitative discussion in Wandel et al. 1999). The breadth of radii across which line-emitting matter is located is one such factor. The angular radiation pattern of the line-emitting material is another.

One way to quantify the radial emissivity distribution is through the “transfer” or “response” function  $\Psi$  defined by

$$\delta L_l(t) = \int_0^\infty d\tau \Psi(\tau) \delta L_c(t - \tau). \quad (1)$$

That is, fluctuations in the continuum luminosity  $\delta L_c$  predict fluctuations in the line luminosity  $\delta L_l$  at later times through a convolution with  $\Psi(\tau)$ . Although the true relationship between line luminosity and incident continuum flux is often nonlinear, if  $\delta L_c$  and  $\delta L_l$  are interpreted as fluctuations relative to a long-term mean value, equation 1 is valid provided the fluctuations are small compared

to the mean. At the order of magnitude level, the amplitude of  $\Psi(\tau)$  tells us how much matter there is (and how sensitive its line output is to continuum fluctuations) at radius  $r \sim c\tau$ . Although relatively few monitoring experiments produced data of good enough quality to allow inferences of  $\Psi(\tau)$  to be made, those that have been analyzed indicate that there is significant response across at least an order of magnitude dynamic range in lag and presumably, therefore, across a comparable dynamic range in radius (Krolik et al. 1991; Done & Krolik 1996; Ulrich & Horne 1996).

This fact means that the characteristic  $r_*$  estimated from comparing the continuum and line light curves is a peculiar weighted average over a wide range of radii. Similarly, the characteristic  $v_*$  is a *different* weighted average of the line-of-sight velocities over that same range. Thus, it is unclear how to interpret the combination  $r_*v_*^2$ , as it mingles contributions from different radii with different weights.

The angular radiation pattern can introduce further factors of order unity because gas at radius  $r$  but on the near side of the continuum source to us appears to respond more quickly than gas at the same radius but on the far side. As we will show in §4.2, the angular radiation pattern also interacts with other sources of systematic error.

Finally, the characteristic scales inferred from monitoring are affected by the shape of the continuum fluctuation power spectrum. The *effective* power spectrum is determined by a combination of the intrinsic spectrum and the details of the particular finite sampling of the experiment because only certain timescales can be probed by an realizable experiment. Because this limitation amounts to a filtering in frequency space, it effectively alters both the line and continuum fluctuation power spectra. Through this means, the sampling also influences the factor  $q$ .

The quantitative impact of these factors (assuming regular sampling and noise-free data) will be examined in detail in §IV. We do not examine the consequences of irregular sampling (which can be expected to introduce a further systematic error) or measurement uncertainty (which introduces a random error). We limit ourselves in this paper to systematic errors because they can be computed very efficiently in the frequency domain; estimating the impact of random errors is far more efficiently done in the time domain because the error at each point in the line profile must be evaluated.

## 2. How Can We Tell That the Dynamics are Gravity-Dominated?

One obvious test of whether the dynamics governing the emission line region are dominated by the gravity of a central point-mass is whether the characteristic speed is  $\propto r^{-1/2}$ . The empirical record here is mixed, but indicates at least marginal consistency with this proposition.

Comparing the cross-correlation peaks of different lines to the widths of their mean profiles as measured in the IUE monitoring campaign on NGC 5548 (Clavel et al. 1991), Krolik et al. (1991) found rough agreement with the relation  $v(r) \propto r^{-1/2}$ . Repeating this exercise with the widths

of the *rms* profiles (for a precise definition, see §4.1), Peterson & Wandel (1999) likewise found consistency, with somewhat smaller departures. Peterson & Wandel (2000) performed the same test on two other galaxies, NGC 7469 and 3C 390.3, again finding consistency, but with poorer data. There are only three data points for NGC 7469 (one of which has rather large uncertainty in  $v_*$ ) and four for 3C 390.3 (with one having large error bars in both  $r_*$  and  $v_*$ ). In both cases, the dynamic range in radius is only a factor of three. On the other hand, Krolik & Done (1996) found that the best fit to the velocity-resolved monitoring data for the CIV 1549 line from the HST campaign on NGC 5548 (Korista et al. 1995) was a rather slower dependence of velocity on radius, although the increased  $\chi^2$  created by forcing  $v \propto r^{-1/2}$  was not large enough to exclude this scaling.

While a significant deviation from  $r^{-1/2}$  scaling could rule out point-mass gravitational dynamics, even perfect agreement could not prove it. The reason is that several other kinds of dynamical models make the same prediction. These include such diverse examples as cloud outflows driven by photoionization when the ionization parameter in the clouds is fixed (Blumenthal & Mathews 1975), disk winds driven by line scattering (Murray et al. 1995), and magnetically-driven disk winds (Emmering, Blandford & Shlosman 1992). In fact, at a qualitative level, both of the latter two models are in rough agreement with the NGC 5548 velocity-resolved monitoring data (Chiang & Murray 1996, Bottorff et al. 1997). In this respect, they are in as good agreement with empirical tests as the model of point-mass gravitational dynamics.

Peterson & Wandel (2000) make the further argument that the mass they infer by assuming gravitational dynamics is so large that the ratio of total luminosity to the Eddington luminosity is too small to permit significant radiative acceleration. This argument is, however, flawed in two important ways.

First, by definition, all rival models have characteristic speeds  $v_*$  that scale  $\propto r^{-1/2}$ . We may therefore write  $v_* = Av_{esc}$ , where, as usual,  $v_{esc} = (GM/r)^{1/2}$ ; if the model entails outflow,  $A \geq 1$ . If that characteristic speed is then used to infer a mass *assuming gravitational dynamics*, the inferred mass will be  $M_{inf} = qv_*^2 r/G = qA^2 M$ . The inferred mass is then an *over-estimate* of the true mass when  $A > 1$ . Because  $M_{inf}/M \propto A^2$ , the error could be substantial.

Second, the correct criterion for driving a radiatively-accelerated wind in emission line gas is not that  $L > L_E$ . Radiation force is proportional to opacity in optically-thin gas, and the Eddington luminosity criterion assumes that the opacity is purely Thomson. In fact, the opacity to ultraviolet and soft X-ray photons presented by gas capable of radiating the observed emission lines can easily be several orders of magnitude greater (this is, in fact, the basis of the radiatively-driven wind models cited earlier).

The values of  $L/L_E$  inferred by Peterson & Wandel (2000) ranged from  $\sim 10^{-3}$  to  $\sim 10^{-1}$ . If  $L_E$  is over-estimated by a factor of 10 (as could easily occur if there are outflows at merely three times the escape speed), the range of  $L/L_E$  inferred shifts to  $\sim 10^{-2} - \sim 1$ . If the effective opacity is  $\sim 10^2$  times greater than Thomson (e.g., from H photoionization opacity in a gas whose H neutral

fraction is  $10^{-4}$  facing a continuum whose peak value of  $\nu L_\nu$  occurs near 10 eV), the inferred ratio of radiation force to gravity ranges from  $\sim 1$  to  $\sim 100$ . Thus, this argument fails to provide any support for dynamics dominated by gravity.

The only further support for broad emission line region dynamics being dominated by the gravity of a central point-mass is the rough agreement found by Gebhardt et al. (2000c) and Ferrarese & Merritt (2000b) between the central mass inferred on the basis of the correlation with the host’s bulge dispersion (Gebhardt et al. 2000b, Ferrarese & Merritt 2000a) and the mass inferred from reverberation by Ho (1999) and Wandel et al. (1999). A similar relationship between the central mass inferred by reverberation mapping and the narrow line width has been found by Nelson (2000).

### 3. The Orbital Shape and Inclination Distribution

If we grant for the sake of argument that the emission line dynamics are due to motion in the potential of a point-mass, it remains to determine the proportionality constant  $q$ . One factor that determines this quantity is the distribution of orbital shape and inclination. To separate these effects from the ones discussed in subsequent sections, suppose for the moment that the material in question emits line radiation only when located a distance  $r$  from the central object. Here, and in the rest of the paper, we will work in terms of the one-dimensional line-of-sight velocity dispersion defined by  $v_*^2 \equiv \langle u^2 \rangle$ , where  $u$  is velocity offset in the line profile and the average is weighted by line flux.

In the simplest imaginable case, all the orbits might be circular (at radius  $r$ ) and confined to a single plane. Then the mean-square line-of-sight velocity is  $(1/2)GM \sin^2 i/r$ , where  $i$  is the inclination angle of the orbital axis relative to the line-of-sight. The factor  $q$  is then  $2/\sin^2 i$ .

On the other hand, it is almost as simple to posit that the velocities are randomly directed. However, we do not know the orbital shapes. Circular orbits have  $|\vec{v}|^2 = GM/r$ , so their mean-square speed in any one direction is  $GM/(3r)$ ; in that case,  $q = 3$ . By contrast, parabolic orbits have  $|\vec{v}|^2 = 2GM/r$ , so that  $q = 3/2$  if they are isotropic.

More complicated models (e.g., supposing that the velocity is a sum of random and planar components as in McLure & Dunlop 2000) are also possible. These, of course, would yield a different correction factor dependent on the ratio of the magnitudes of the two components as well as on the inclination angle. Efforts to infer nuclear masses from stellar kinematics have found it necessary to employ extensive modeling in order to determine how the uncertainty in orbital shape distribution contributes to uncertainty in the inferred mass (e.g., Gebhardt et al. 2000a). Similar complexities may also apply here.

We have now found that values of  $q$  predicted by equally simple models range all the way from a minimum of  $3/2$  to a maximum (nominally) of infinity, in the event of a thin orbital plane

perpendicular to the line-of-sight. Although a very thin orbital plane is a bit implausible, thicknesses of  $\sim 10^{-1}$  cannot yet be easily ruled out. If so, the range of uncertainty for  $q$  from considerations of orbital shape alone is two orders of magnitude, from  $3/2$  to  $\sim 200$ .

We conclude this section with a technical note. Not all authors define  $v_*$  as the root-mean-square speed. Some measure the FWHM of the profile instead. If the profile is Gaussian with dispersion  $\sigma$ , these quantities are related by the expression  $v_{FWHM} = 2\sqrt{2\ln 2}\sigma = 2.35\sigma$  (cf. the expression  $v_{FWHM} = (2/\sqrt{3})\sigma_{3d}$  suggested by Netzer 1990 and used by Wandel et al. 1999 and Peterson & Wandel 2000; note that the inferred mass scales as the square of this conversion coefficient).

## 4. The Radial Emissivity Distribution

### 4.1. What Kinds of Moments are $r_*$ and $v_*$ ?

To describe the way in which the characteristic scales depend on the radial emissivity distribution, we begin with the velocity-dependent response function

$$\Psi(\tau, u) = \int dV \frac{1}{4\pi r^2} \frac{\partial j}{\partial F_{ion}}(\vec{r}) \Phi(\hat{r} \cdot \hat{z}) \delta[\tau - \tau(\vec{r})] \int d^3v f(\vec{v}, \vec{r}) \delta(u - \vec{v} \cdot \hat{z}), \quad (2)$$

where  $j$  is the local line emissivity,  $\hat{z}$  is the direction of the line-of-sight,  $\tau(\vec{r}) = (r/c)(1 - \hat{r} \cdot \hat{z})$  is the time lag corresponding to position  $\vec{r}$ ,  $\Phi$  describes the angular radiation pattern of the emission (we assume that it is oriented with respect to  $\hat{r}$ ), and  $f(\vec{v}, \vec{r})$  is the velocity distribution function at  $\vec{r}$ . As we will discuss at greater length later in this paper, it is desirable to define  $r_*$  and  $v_*$  so that they correspond, as much as possible, to the same material. For this reason, we will use, as recommended by Peterson & Wandel (1999), the variable part of the line to measure the velocity moment as well as the characteristic lengthscale.

Several different empirical definitions of  $r_*$  have been used, but all make use of the line-continuum total-flux cross-correlation function  $C_{lc}$ . For example, some have used the peak of  $C_{lc}$ , whereas Wandel et al. (1999) and Kaspi et al. (2000) employed the centroid of that portion of  $C_{lc}$  whose amplitude is at least 80% of the peak amplitude. Written in terms of  $\Psi$ , the cross-correlation function is

$$C_{lc}(\tau) = \frac{1}{\sigma_l \sigma_c} \int du \int dt \Psi(u) * \delta F_c \delta F_c(t - \tau), \quad (3)$$

where  $\sigma_{l,c}$  are the *rms* fluctuations in the line and continuum flux,  $F_c(t)$  is the continuum flux at time  $t$ , and “\*” denotes a convolution. The dependence of  $C_{lc}$  on the continuum fluctuation power spectrum is more clearly displayed when it is written in terms of Fourier-transformed quantities:

$$C_{lc}(\tau) = \int du \int df e^{-2\pi i f \tau} \hat{\Psi} |\delta \hat{F}_c|^2, \quad (4)$$

where  $\hat{\cdot}$  over a symbol (except for  $\hat{z}$ , the unit vector) indicates a Fourier transform. Because  $\Psi(\tau)$  is a real function, it is convenient to rewrite this expression as

$$C_{lc}(\tau) = \int du \int_0^\infty df 2\text{Re} \left[ e^{-2\pi i f \tau} \hat{\Psi} \right] |\delta \hat{F}_c|^2. \quad (5)$$

If  $\tau_*$  is defined as a centroid of the cross-correlation function, we have

$$\tau_* = \frac{\int d\tau \tau \int du \int_0^\infty df 2\text{Re} \left[ e^{-2\pi i f \tau} \hat{\Psi} \right] |\delta \hat{F}_c|^2}{\int d\tau \int du \int_0^\infty df 2\text{Re} \left[ e^{-2\pi i f \tau} \hat{\Psi} \right] |\delta \hat{F}_c|^2}, \quad (6)$$

where the limits on the  $\tau$  integrals are chosen according to the particular kind of centroid desired.

Similarly,  $v_*$  may be defined in any of several ways, all based on the *rms* profile. As discussed in §III, some use its FWHM, others its mean-square speed. Writing the *rms* profile also in terms of  $\hat{\Psi}$  and  $\delta \hat{F}_c$ , we have

$$F_{rms}(u) = \left[ T^{-1} \int_0^T dt |\Psi(u) * \delta F_c|^2 \right]^{1/2} \quad (7)$$

$$= \left[ T^{-1} \int df |\hat{\Psi} \delta \hat{F}_c|^2 \right]^{1/2}, \quad (8)$$

where the second form follows from the convolution and Parseval's theorems. If, for example,  $v_*$  is defined as the *rms* speed,

$$v_* = \left\{ \frac{\int du u^2 \left[ T^{-1} \int df |\hat{\Psi} \delta \hat{F}_c|^2 \right]^{1/2}}{\int du \left[ T^{-1} \int df |\hat{\Psi} \delta \hat{F}_c|^2 \right]^{1/2}} \right\}. \quad (9)$$

Contrasting equations 6 and 9 makes it clear that the moments over the radial distribution resulting in  $r_*$  and  $v_*$  are *different*, so that the characteristic scales they refer to need not coincide. These forms also make it obvious that the moments depend on  $\delta \hat{F}_c$  in addition to the intrinsic nature of the emission line region.

In the preceding derivation we have tacitly assumed that an infinite amount of data is available to determine the cross-correlation function and *rms* line profile. Real experiments do not, of course, yield infinite data trains. However, the pairing between function and Fourier transform can be taken over almost without alteration to discrete Fourier transforms after allowance for a few restrictions: the functions are assumed to be periodic with a period equal to the duration  $T$  of the data; the sampling is uniform (we call the interval  $\Delta t$ ); the limits on frequency in all integrals are  $-1/(2\Delta t)$  to  $+1/(2\Delta t)$ ; and the frequency resolution is  $1/T$ .

One consequence of these restrictions is that the data are effectively filtered in such a way as to eliminate all frequencies higher than  $1/(2\Delta t)$  and lower than  $1/T$ . In rough terms, there is a mapping between frequency  $f$  and distance-scale  $r \sim c/f$ ; therefore, the character of the sampling can bias the weighting given different distance-scales, ultimately leading to a systematic error in the inferred mass.

## 4.2. Examples

To explore the impact of these moments, we have used equations 6 and 9 to evaluate  $M_{inf}/M$  for a variety of choices of continuum variability behavior, underlying physical model, and sampling. Our goal is to separately identify the systematic errors induced by each cause: intrinsic character of the moments, detailed properties of the line emission such as angular radiation pattern or radial distribution, and poor sampling.

### 4.2.1. Model definition

In all cases, we will use the same basic model, chosen as the simplest non-trivial one permitting an exploration of these effects. In this model the line emissivity depends only on  $r$ , the angular radiation pattern  $\Phi(\mu) = (1 - \mu)^\gamma$  for  $\gamma = 0$  or  $1$  (here  $\mu \equiv \hat{r} \cdot \hat{z}$ ), and the 1-d velocity distribution is a Gaussian with dispersion  $v(r)$ . So that effects due to orbital shape and inclination may be cleanly separated from the other sources of systematic error, we assume in all cases that  $v(r) = (GM/3r)^{1/2}$ , i.e., the orbits are circular and isotropically-oriented. This choice implies that the correct value of  $q$  is  $3M/M_{inf}$ . The response function  $\Psi$  is then

$$\Psi(\tau, u) = \int_{c\tau/2}^{\infty} dr \frac{c}{2r} \frac{\partial J}{\partial F_{ion}}(r) \frac{e^{-u^2/[2v^2(r)]}}{[\pi v^2(r)]^{1/2}} \Phi(1 - c\tau/r). \quad (10)$$

Here  $J \equiv \int d\Omega r^2 j$ , i.e., the radial emissivity distribution.

For the purpose of computing  $\hat{\Psi}$ , it is convenient to reverse the order of the  $r$  and  $\tau$  integrations, i.e.,

$$\hat{\Psi}(f, u) = \int_0^{\infty} dr \frac{c}{2r} \frac{\partial J}{\partial F_{ion}}(r) \frac{(c/r)^\gamma}{\sqrt{2\pi}v(r)} e^{-u^2/[2v^2(r)]} \int_0^{2r/c} d\tau \tau^\gamma e^{2\pi i f \tau}. \quad (11)$$

For any integral value of  $\gamma$ , the  $\tau$  integral is easy to evaluate analytically.

It is now time to choose a physical model. We have two goals: exploring the consequences of radial distributions that have a range of radial widths, and being at least crudely consistent with what we have learned from detailed studies of the response functions of selected AGN (Krolik et al. 1991; Horne et al. 1991; Wanders et al. 1995; Done & Krolik 1996; Ulrich & Horne 1996). Dependence on the width of the radial distribution is of special interest because there are indications from these detailed studies that the true radial distribution may in fact span an order of magnitude or more in radius. Towards that end, we write

$$\frac{\partial J}{\partial F_{ion}} = J_o \exp \left[ -(\log r - \log r_o)^2 / (\Delta \log r)^2 \right], \quad (12)$$

where  $J_o$  is an (arbitrary and irrelevant) constant,  $r_o$  is the center of the distribution of line emissivity with respect to radius, and  $\Delta \log r$  is its characteristic width in terms of  $\log_{10} r$ . We stress, however, that there are substantial uncertainties in the emissivity distributions that have

been measured, and these measurements exist for only a handful of objects; we therefore know very little about the true range of possibilities. For this reason, these simulations must be regarded as purely illustrative; real AGN may have much more complicated emissivity distributions.

We also assume for the simulations reported here that the power density spectrum of continuum fluctuations takes a power-law form:  $|\delta\hat{F}_c|^2 \propto f^{-n}$ . We have explored the consequences of varying  $n$ , and find that in most instances it changes the results in only a minor way. As a result of these preliminary explorations, we decided to fix  $n = 1.5$  for all the calculations reported in this paper.

Finally, we define  $r_*$  as the centroid of the portion of the cross-correlation curve whose amplitude is greater than 80% of the peak, except in those cases in which the 80% level lies beyond the range of lags where the cross-correlation may be estimated—in those cases (which are few), we use the cross-correlation peak to define the characteristic radius.

#### 4.2.2. *Errors due to the moments and the underlying physics*

We begin by defining the systematic errors due solely to the differing moments. These are defined by assuming an “ideal” experiment, i.e. one with 900 measurements spaced at an interval  $\Delta t = (1/30)(r_o/c)$ . Two examples are illustrated in Figure 1, one assuming isotropic radiation, the other assuming  $\Phi \propto 1 - \mu$ . As can be seen, in both cases the inferred mass is biased towards values larger than the true value, but by rather more in the anisotropic radiation case. The reason for this distinction is clear: When we preferentially see regions on the far side of the center, the lag is greater than what it would be if we could see all the emitting regions. Thus, the estimated  $r_*$  is also greater than it should be, and the estimated mass likewise because  $M_{inf} \propto r_*$ . In both cases, the bias grows with increasing width of the radial emissivity distribution. The reason for this, too, is easy to see: differing moments mean little when the underlying distribution is narrow. For the widest distribution we consider ( $\Delta \log r = 1.5$ ), the error is 60% in the isotropic case, and a factor of 2.7 in the anisotropic case. The method, therefore, has an *intrinsic* bias toward overestimating the central mass that can be small in favorable cases (sharply peaked radial emissivity distributions) but considerably larger in unfavorable ones.

#### 4.2.3. *Errors due to sampling*

Next we examine the effects of sampling, beginning with experiments that are “as good as can be hoped”. We define this phrase as denoting an experiment with 64 sampling points and interval  $\Delta t = (1/8)(r_o/c)$ . Judging by the history of the experiments, this seems to be about as many measurements as can be managed (e.g., 60 were obtained in the original IUE campaign: Clavel et al. 1991; 39 were obtained in the HST campaign on NGC 5548: Korista et al. 1995; of the 28 quasars monitored by Kaspi et al. 2000, the median number of observations was 25, although one had as many as 70).

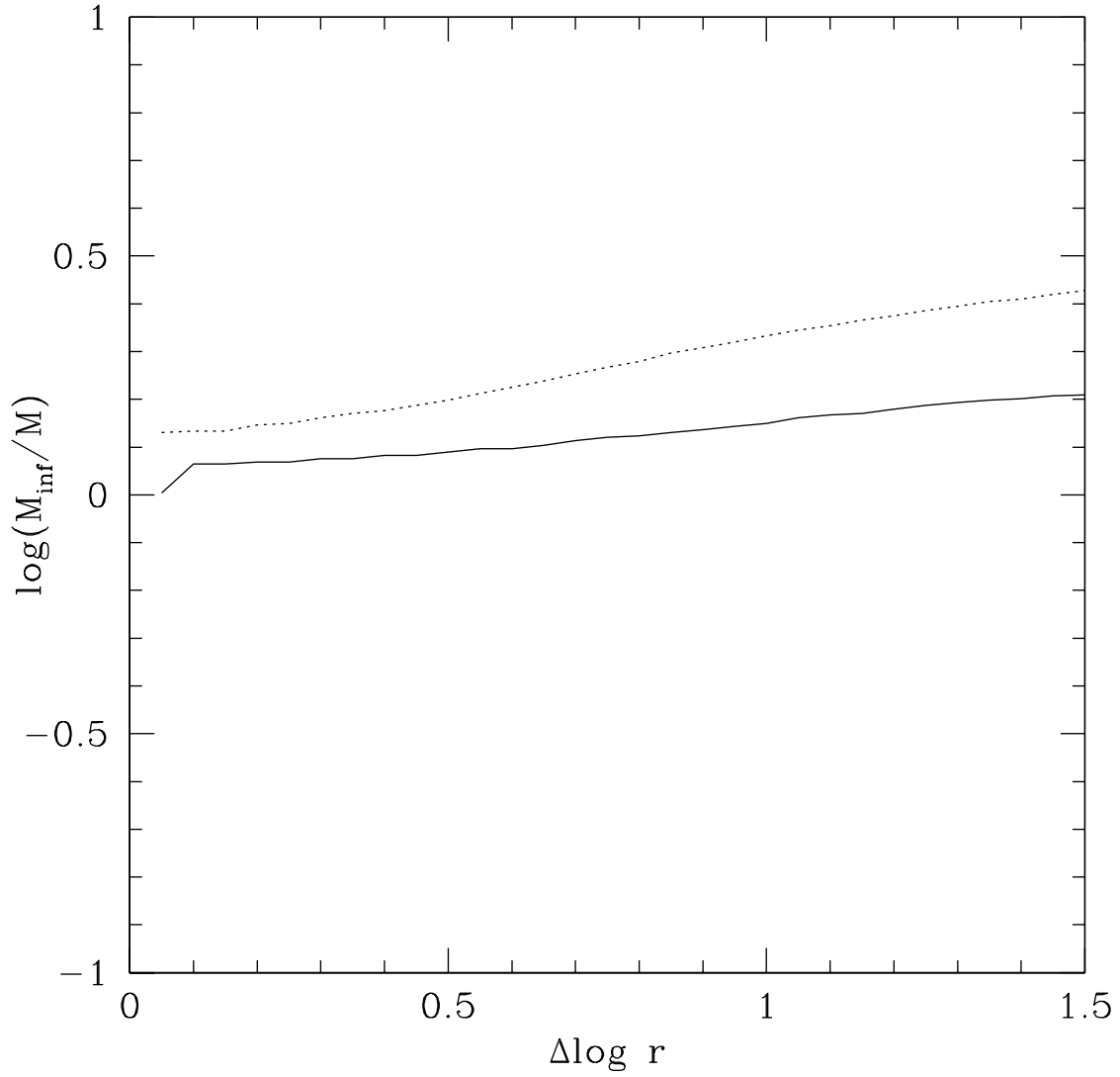


Fig. 1.— Systematic error due solely to the differing moments that define  $v_*$  and  $r_*$ . The solid curve refers to isotropic radiation, the dotted to  $\Phi \propto 1 - \mu$ .

The expected level of systematic error from experiments “as good as can be hoped” is shown in Figure 2. Contrasting that figure to Figure 1, we see that when the emission is anisotropic in the sense chosen, the reduction in sampling makes almost no difference at all. Surprisingly, “good”, but less than “ideal”, sampling actually *decreases* the level of systematic error in the case of isotropic radiation. We will learn the reason for this when we study poorer sampling.

Truly sub-optimal sampling increases the opportunity for error. Two kinds of problems are possible. The first kind is a simple shortage of data. Instead of having 64 measurements, as in the “as good as can be hoped” example, there might be many fewer. The consequences of data sets that are too small are shown in Figure 3. As that figure shows, there is a systematic bias produced by short data sets toward smaller values of  $M_{inf}/M$ . When the radial distribution is narrow, the bias is small because only a narrow range of timescales occurs in the data. However, as the radial distribution becomes broader, the effect grows. Because the contrasting moments entering into  $M_{inf}$  create a systematic shift toward  $M_{inf}/M > 1$  for large  $\Delta \log r$ , the statistical bias of short data trains can partially counteract the systematic error induced by the moments. It is then possible for the net systematic error to be fortuitously small.

The second kind of deviation from optimal sampling is an offset in timescales sampled. When planning a monitoring experiment, one does not know in advance what the characteristic size of the emission line region is, although one might estimate it by scaling from other examples (e.g., by supposing that  $r_o \propto L^{1/2}$ , as might be expected on the basis of simple photoionization models; but see the doubts raised by Kaspi et al. 2000). Offsets in the sampling interval relative to  $r_o/c$  are therefore quite likely. We define  $\phi = (T\Delta t)^{1/2}c/r_o$  as the offset parameter; when  $\phi < 1$ , the scales sampled are too small, when  $\phi > 1$ , they are too large. Figure 4 illustrates the impact of a factor of 3 error even when a substantial data set is obtained.

Larger offsets can create still larger errors. After exploring the range  $0.01 < \phi < 100$ , we find that when the radiation is isotropic,  $M_{inf}/M \simeq s(\phi, \Delta \log r)\phi$ , where  $s$  is a slowly-varying function of  $\phi$ , such that

$$s(\phi, \Delta \log r) \simeq \begin{cases} 1 & \phi < 1, \Delta \log r \ll 1 \\ 3 & \phi < 1, \Delta \log r > 1 \\ 0.25 & \phi > 1, \Delta \log r \ll 1 \\ 0.2 & \phi > 1, \Delta \log r > 1 \end{cases} \quad (13)$$

Anisotropic radiation leads to more complicated behavior. Values of  $\phi$  between 0.1 and 10 bias the result toward  $M_{inf}/M$  smaller than unity (for  $\phi < 1$ ) and  $M_{inf}/M$  greater than unity (for  $\phi > 1$ ), but by smaller amounts than in the isotropic case. More extreme values of  $\phi$  push the bias sharply in either direction, smaller values of  $\phi$  leading to greatly underestimated masses and larger values to numbers that are substantial overestimates. Unfortunately, unlike the case of isotropic radiation, there is no simple approximate expression that encapsulates these dependences.

The origin of the sensitivity of  $M_{inf}/M$  to  $\phi$  lies in the mismatch that is created when  $\phi$  is grossly different from unity between the natural timescales of the system and the timescales probed

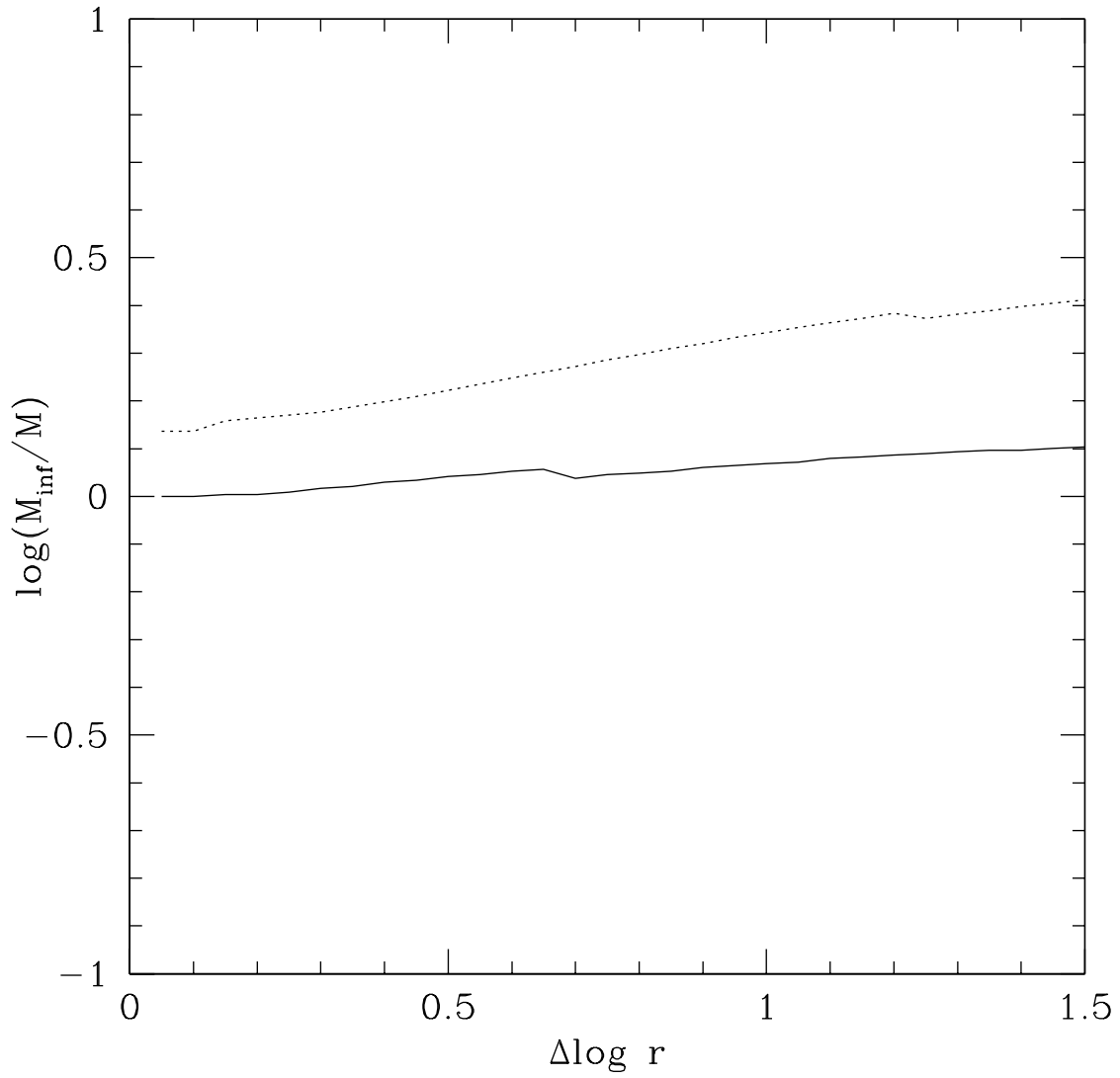


Fig. 2.— Systematic error as a function of  $\Delta \log r$  in the case of “as good as can be hoped” sampling. The solid curve refers to isotropic radiation, the dotted to  $\Phi \propto 1 - \mu$ .

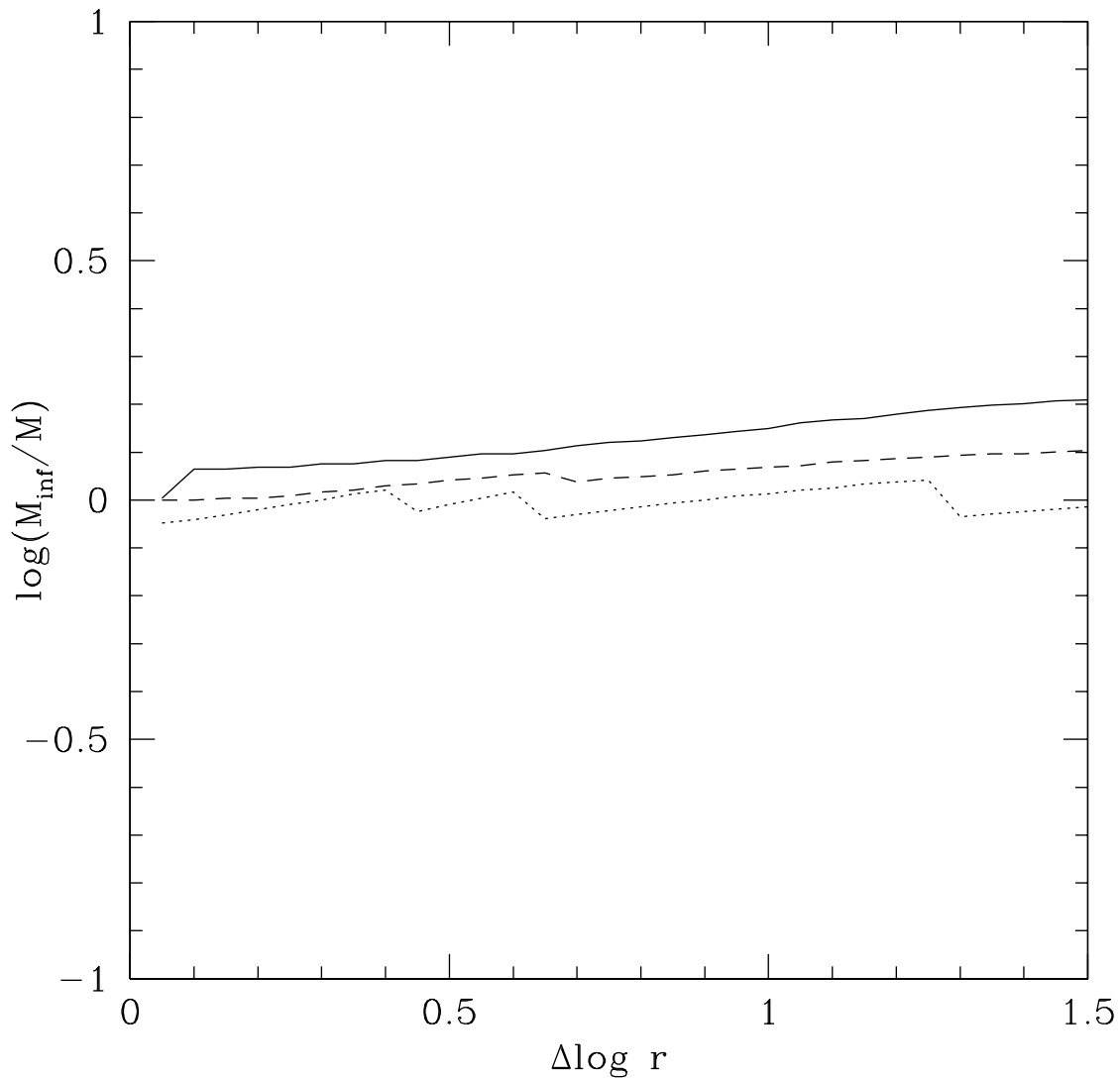


Fig. 3.— Systematic error as a function of  $\Delta \log r$  for several different length experiments, all with timescales centered on  $r_o/c$ , and assuming isotropic radiation in each case. The solid line is the result of 900 data points, the dashed line is the product of 64 measurements, and the dotted line comes from a simulated experiment with only 25 points.

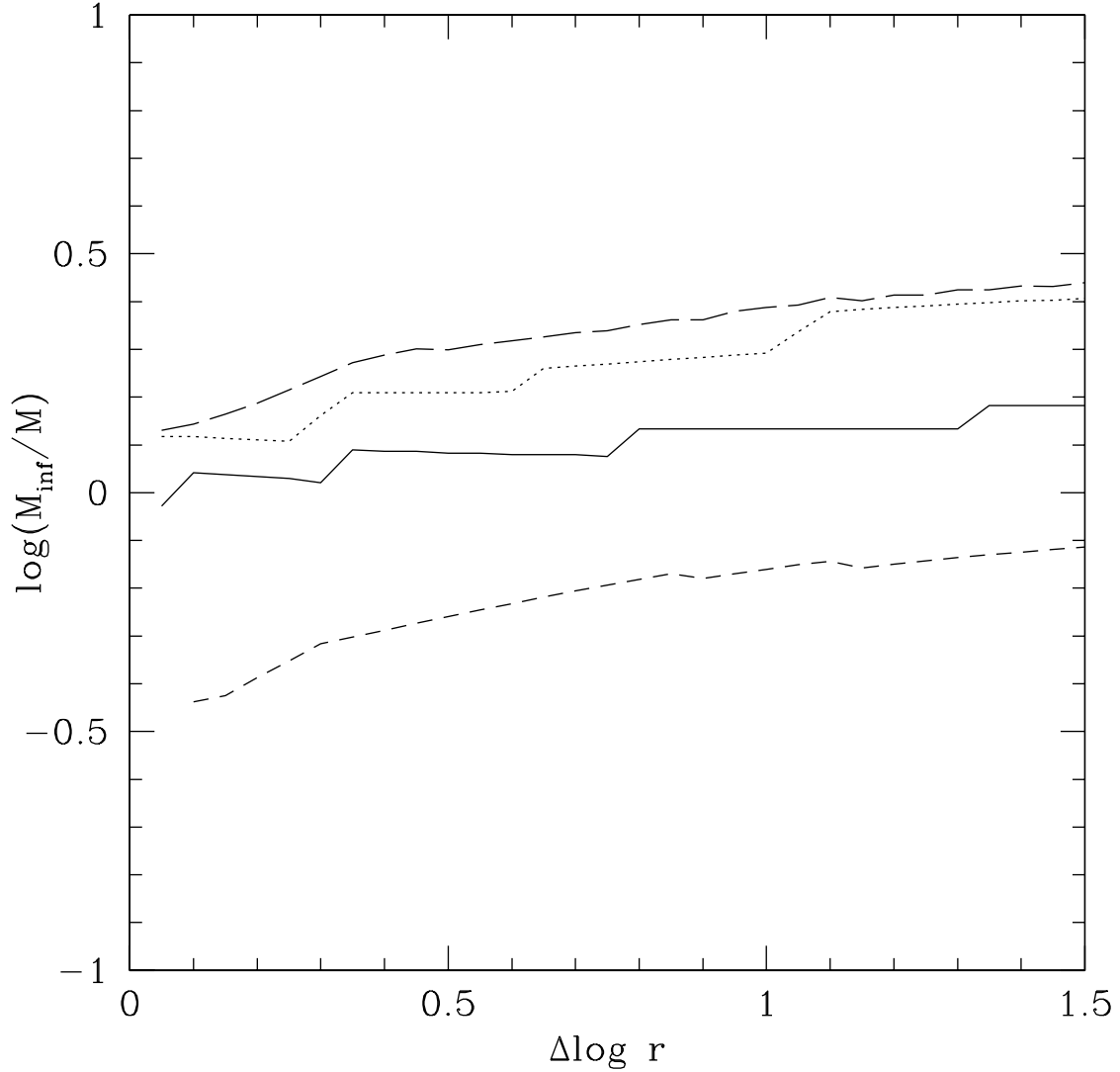


Fig. 4.— The ratio  $M_{inf}/M$  as a function of  $\Delta \log r$  for four experiments with a large number of points (64), but different sampling intervals. The solid curve pertains to isotropic radiation and  $\Delta t = (3/8)(r_o/c)$ ; the dashed curve shows the result for the same model but with  $\Delta t = (1/24)(r_o/c)$ . The dotted and long-dashed curves pertain to a model with  $\Phi \propto 1 - \mu$ ;  $\Delta t = (3/8)(r_o/c)$  for the dotted curve, while  $\Delta t = (1/24)(r_o/c)$  for the long-dashed curve. The jagged breaks, which are particularly noticeable in the solid curve, are due to the relatively small number of points contributing to the cross-correlation centroid integrations.

by the experiment. As a result, the peak in the profile-integrated cross-correlation function can be severely biased: for example, in the case of isotropic radiation and  $\phi = 0.01$ , the characteristic scale derived from the cross-correlation centroid is  $\simeq 0.01$  times what it is when the sampling is perfectly matched to the true scales. That there is a peak anywhere in the measurable range of lags is due to the existence of some matter close to the line of sight, where it can respond quickly despite its distance from the central source; by contrast, in the case of  $\Phi \propto 1 - \mu$ , for which matter on the line of sight is essentially invisible, the cross-correlation function is greatest at the largest lag measurable. Because the *rms* line profile is much less strongly affected by sampling problems, the bias in the mass estimate corresponds very nearly to the bias in the characteristic distance scale estimate. Not surprisingly, tight radial distributions (i.e., small values of  $\Delta \log r$ ) exacerbate the timescale mismatch effect, but relatively weakly compared to the much larger bias driven by the poor sampling.

## 5. Discussion

### 5.1. Deciding Whether the Black Hole’s Gravity Dominates Emission Line Dynamics

Measuring central black hole masses by the reverberation method is possible only if gravity dominates the dynamics of the line-emitting gas and the mass of the black hole is much larger than any other mass within the line-emitting region. As was shown in §2, the evidence in hand to date neither proves nor disproves this assumption. The question naturally arises as to how this situation might be clarified.

Point-mass gravitational dynamics might be discredited if evidence arose showing that  $v$  did not scale as  $r^{-1/2}$ . One possible way to do so would be to conduct experiments like the HST campaign on NGC 5548, but with better data, so that  $\Psi(\tau, u)$  could be more tightly constrained. “Better” in this context means more epochs of observation and a combination of better signal/noise and velocity resolution. More epochs of observation serves both to reduce statistical scatter and to create a larger dynamic range in timescales (and hence length scales) probed. Better signal/noise and velocity resolution would permit dividing the line profile into more segments in order to achieve a greater dynamic range in  $u$ .

However, demonstrating consistency with  $v \propto r^{-1/2}$  is not sufficient to prove that the black hole’s gravity controls the dynamics of line-emitting gas because there are other models that make the same prediction. Testing these other models vis-a-vis point-mass gravity requires independent methods. Disk winds might be tested by searching for the correlation between radial and azimuthal velocity that they generically predict (Chiang & Murray 1996). Although this prediction is qualitatively consistent with the relatively rough constraints posed by the HST campaign on NGC 5548, an improved experiment of the sort described in the previous paragraph might sharpen this test. Nonetheless, because the kinematic predictions of so many models are so similar, providing a direct

proof of gravity-dominated dynamics will be difficult.

## 5.2. Systematic Errors Granted Gravitational Dynamics: Magnitude and Mitigation

If, for the sake of argument, we grant the assumption that the motions of the line-emitting gas are dominated by response to the black hole’s gravity, both random and systematic errors of several different varieties may cloud the result. In this paper, we have concentrated on the *systematic* errors.

One sort is due to our ignorance of the orbital shapes. Changing from parabolic to circular orbits alters the inferred mass by a factor of two. Even if the orbital eccentricity distribution is known, flattening of the emission line region can introduce a new systematic error by eliminating our ability to average over the velocity vectors’ projections on the line-of-sight. This error can be as large as  $\sim (r/h)^2$  for aspect ratio  $h/r$ . In principle, this latter effect could produce a very large error.

Unfortunately, whether the broad line region is round, flat, or some other shape is still a controversial issue (Wanders et al. 1995, Dumont et al. 1998). It is even possible that the region responsible for some lines (e.g., the high-ionization lines like CIV 1549) is round while the region radiating the Balmer lines is flattened (Rokaki et al. 1992).

Another variety of systematic error arises from the interaction between the differing ways in which  $r_*$  and  $v_*$  depend on the response function, the details of the radial emissivity distribution, the angular radiation pattern, and the sampling. Although in some sense each of these contributions is logically independent, the magnitude of the combined error cannot be estimated by simply adding them in quadrature. For example, if the line radiation is isotropic, relatively little systematic error is induced by the character of the moments defining  $r_*$  and  $v_*$ , wide emissivity distributions, or meager datasets; on the other hand, the results obtained when the line radiation is isotropic are very sensitive to the characteristic sampling timescale. However, it should also be borne in mind that all of these conclusions were reached on the basis of exploring a very simple emissivity model; more complicated geometries might well lead to new dependences for the systematic errors.

The central problem, of course, is that with only a single monitoring dataset it is difficult to determine which of these characteristics apply to any particular quasar or line. Although most photoionization models (e.g., Kwan & Krolik 1981, Ferland et al. 1992) predict that H recombination lines are emitted rather anisotropically (more or less in the sense described by  $\Phi \propto 1 - \mu$ ), we can hardly claim to know this reliably (for an example of complications that might change this prediction, see Kallman & Krolik 1986). It is possible that other lines are also emitted anisotropically, but this suggestion is even more model-dependent (Ferland et al. 1992, O’Brien et al. 1994). Similarly, we do not know anything *a priori* about the geometric symmetry of the emission line region or the radial dependence of emissivity within it. At the same time, as the curves of Figure 2 illustrated, it is also possible for systematic errors to cancel fortuitously. Consequently, although

we may hope that conditions are such that the systematic error is small, it is hard at this stage to be confident.

A partial step forward could be provided by a two-step process applied to each target object individually: First, the breadth and characteristic scale of the radial emissivity distribution can be estimated by monitoring that spans a truly broad range of timescales; this experiment does not require good quality spectral resolution. Second, with that knowledge in hand, it would be possible to design a new experiment with optimized sampling and spectral resolution that might be better able to control those systematic errors due to inappropriate sampling scale or ignorance of the radial emissivity distribution.

Another partial advance could come from making fuller use of the information obtained in emission line monitoring experiments. In the efforts to estimate  $M$  so far, only the moments  $r_*$  and  $v_*$  have been used. There is potentially much more information contained in the full set of time-dependent line profiles. If good enough data were obtained that  $\Psi(\tau, u)$  could be accurately determined, many (although not all) of these uncertainties could be either eliminated or constrained. For example, as we have already remarked, the central assumption that  $v \propto r^{-1/2}$  could be tested directly. At a more detailed level, different orbital shape and inclination distributions can be distinguished by the contrasting shapes they give  $\Psi$  in the  $\tau$ - $u$  plane (Welsh & Horne 1991). Although  $\Psi(\tau, u)$  does involve an integration over radius (as in equation 10, for example), it still provides some indication of the radial emissivity distribution.

### 5.3. Random Errors

We stress that in this paper we have discussed only *systematic* errors. Random errors arising from flux measurement uncertainties and the fluctuations due to specific realizations of the random processes involved add to the final uncertainty (Peterson et al. 1998; Welsh 1999).

### 5.4. Conclusions

Given all these considerations, it would seem that, taken in isolation, there are systematic uncertainties in the estimation of black hole masses by the reverberation method that are potentially large, but whose magnitudes are difficult to estimate quantitatively. In order to gain confidence in the results obtained by this method, further efforts to control these systematic errors are essential.

Unfortunately, the underlying question of whether gravity truly dominates the dynamics is particularly difficult to answer securely and is rendered more difficult by the existence of uncontrolled systematic errors. If other, independent, measurements yield black hole masses that coincide with those inferred from reverberation mapping (as seems possible: Gebhardt et al. 2000c; Ferrarese & Merritt 2000b), this agreement might be taken as evidence in support of gravitational dynamics in

the broad line region. Until we understand these systematic errors better, however, it still remains possible that such agreement could be merely the result of a fortuitous cancellation of systematic errors.

Consider one example of how this might come about: As described in §2, many models in which non-gravitational dynamics dominate predict a characteristic speed that scales with the escape speed. If the emission line kinematics are interpreted as gravitational, the mass is then consistently overestimated by a fixed ratio. A systematic measurement error that underestimates the mass (as would be induced by a characteristic sampling time that is too short applied to an isotropically-radiated emission line) could then produce an entirely fortuitous agreement. We would then be in the odd position of arriving at the correct mass, but only as a result of mutually cancelling errors.

I thank Eric Agol, Tim Heckman, and Jerry Kriss for many helpful conversations and suggestions. This work was partially supported by NSF Grant AST-9616922.

## REFERENCES

- Blumenthal, G.R. & Mathews, W.G. 1975, *ApJ* 198, 517
- Bottorff, M., Korista, K.T., Shlosman, I. & Blandford, R.D. 1997, *ApJ* 479, 200
- Chiang, J. & Murray, N. 1996, *ApJ* 466, 704
- Clavel, J. et al. 1991, *ApJ* 366, 64
- Collier, S. et al. 1998, *ApJ* 500, 162
- Done, C. & Krolik, J.H. 1996, *ApJ* 463, 144
- Dumont, A.-M., Collin-Souffrin, S. & Nazarova, L. 1998, *A&A* 331, 11
- Edelson, R.A. & Krolik, J.H. 1988, *ApJ* 333, 646
- Emmering, R.T., Blandford, R.D. & Shlosman, I. 1992, *ApJ* 385, 460
- Ferland, G.J., Peterson, B.M., Horne, K., Welsh, W.F. & Nahar, S.N. 1992, *ApJ* 387, 95
- Ferrarese, L. & Merritt, D. 2000a, *ApJ* 539, L9
- Ferrarese, L. & Merritt, D. 2000b, *astro-ph/0008310*
- Gebhardt, K. et al. 2000a, *AJ* 119, 1157
- Gebhardt, K. et al. 2000b, *ApJ* in press, *astro-ph/0006289*

- Gebhardt, K. et al. 2000c, astro-ph/0007123
- Gondhalekar, P.M., Horne, K. & Peterson, B.M. 1994, Reverberation Mapping of the Broad-Line Region in Active Galactic Nuclei (San Francisco: Astronomical Society of the Pacific)
- Ho, L. 1999, in Observational Evidence for Black Holes in the Universe, ed. S.K. Chakrabarti (Dordrecht: Kluwer), 157
- Horne, K.D., Welsh, W.F. & Peterson, B.M. 1991, ApJ 367, L5
- Kallman, T.R. & Krolik, J.H. 1986, ApJ 308, 805
- Kaspi, S., Smith, P.S., Netzer, H., Maoz, D., Jannuzzi, B.T. & Giveon, U. 2000, ApJ 533, 631
- Korista, K.T. et al. 1995, Ap. J. Suppl. 97, 285
- Krolik, J.H., Horne, K.D., Kallman, T.R., Malkan, M.A., Edelson, R.A. & Kriss, G.A. 1991, ApJ 371, 541
- McLure, R.J. & Dunlop, J.S. 2000, astro-ph/0009406
- Murray, N., Chiang, J., Grossman, S. & Voit, G.M. 1995, ApJ 451, 498
- Nelson, C.H. 2000, astro-ph/0009188
- Netzer, H. 1990, in Active Galactic Nuclei: 1990 Saas-Fee Lectures, eds. T.J.-L. Courvoisier and M. Mayor (Berlin: Springer-Verlag)
- O'Brien, P.T., Goad, M.R. & Gondhalekar, P.M. 1994, MNRAS 268, 845
- Peterson, B.M. et al. 1998, P.A.S.P. 110, 660
- Peterson, B.M. & Wandel, A. 1999, ApJ 521, L95
- Rokaki, E., Boisson, C. & Collin-Souffrin, S. 1992, A&A 253, 57
- Ulrich, M.-H. & Horne, K.D. 1996, MNRAS 283, 748
- Wandel, A. 1999, ApJ 519, L39
- Wandel, A., Peterson, B.M. & Malkan, M.A. 1999, ApJ 526, 579
- Wanders, I. et al. 1995, ApJ 453, L87
- Welsh, W.F. 1999, P.A.S.P. 111, 1347
- Welsh, W.F. & Horne, K.D. 1991, ApJ 379, 586